Spring 5-9-2020

Synthesis and Characterization of Transition Metal Scorpionate Complexes for Redox Shuttle Applications in Dye-Sensitized Solar Cells

Chase Lance

Synthesis and Characterization of Transition Metal Scorpionate Complexes for Redox Shuttle Applications in Dye-Sensitized Solar Cells

by

Chase M. Lance

A thesis submitted to the faculty of the University of Mississippi in partial fulfillment of the requirements for the Sally McDonnell Barksdale Honors College

Oxford

May 2020

Approved by

_____

Advisor: Dr. Jonah Jurss

_____

Advisor: Dr. Walter Cleland

_____

Reader: Dr. Jared Delcamp

Acknowledgements

I would like to thank Dr. Walter Cleland for his guidance and wisdom during the time I spent in his laboratory. I would also like to thank Dr. Jonah Jurss for his endearing passion as my advisor for the year I was a member in his group. Both advisors were an invaluable resource who consistently mentored and motivated me to strive for excellence. I was able to study and immerse myself in the field of chemistry, obtaining an unimaginable skillset. I would also like to thank the graduate students in my research group for their willingness to assist and further my knowledge in chemistry. Finally, I sincerely appreciate the Sally McDonnell Barksdale Honors College for this demanding and fascinating experience as well as the funding for this project.

Abstract

Given the rising global energy demands, alternative renewable energy sources are currently being investigated. The most appealing renewable energy source is solar energy, and dye-sensitized solar cells (DSSCs) in particular are an attractive technology. DSSCs have traditionally utilized iodide/triiodide as the redox mediator couple, which exhibits high efficiencies and fast regeneration of the oxidized dye with little recombination. Recently, the use of alternative redox couples based on transition metal complexes has been studied as a promising substitute due to the tunable design of these complexes. In this study, tridentate tris(pyrazolyl)borate and tris(pyrazolyl)methane ligands with first-row transition metals were designed and synthesized to function as viable redox shuttles in DSSCs. Electrochemical studies of these complexes exhibit reversible redox couples within the desired parameters for DSSCs. The synthesized first-row transition metal tris(pyrazolyl)borate complexes demonstrate electrochemical reversibility, but lack the desired solubility in acetonitrile. Due to the minimal solubility of the Tp complexes, the study shifts focus to Tpm complexes for this DSSC application. Indeed, the $[Fe(Tpm)_2]^{3+/2+}$ system exhibits both electrochemical reversibility and the desired solubility in acetonitrile, making it a promising redox shuttle candidate. Future work to test the $[Fe(Tpm)_2]^{3+/2+}$ system in a DSSC is needed to determine the viability of this redox shuttle in a working device. Overall, this study illustrates that the synthesized iron Tpm complexes could be a viable alternative to the traditional I^-/I_3^- electron mediator, but further testing is necessary to establish the efficiency.

Table of Contents

1. Introduction

1.1: Global Energy Demands

There has been an exponential rise in the consumption of energy on a global scale since the early 1900's. In the United States alone, the sources of energy have shifted from the renewable resource of wood to fossil fuels, such as petroleum, coal, and natural gas. The transition to fossil fuels is illustrated in **Figure 1** for the United States over a 234-year period. While various forms of energy sources are combating this growing energy demand, the majority of the energy needs are met with fossil fuels. In particular, the fossil fuels of coal, petroleum, and natural gas have accounted for 87% of the total U.S. energy consumption over the past decade.[1]

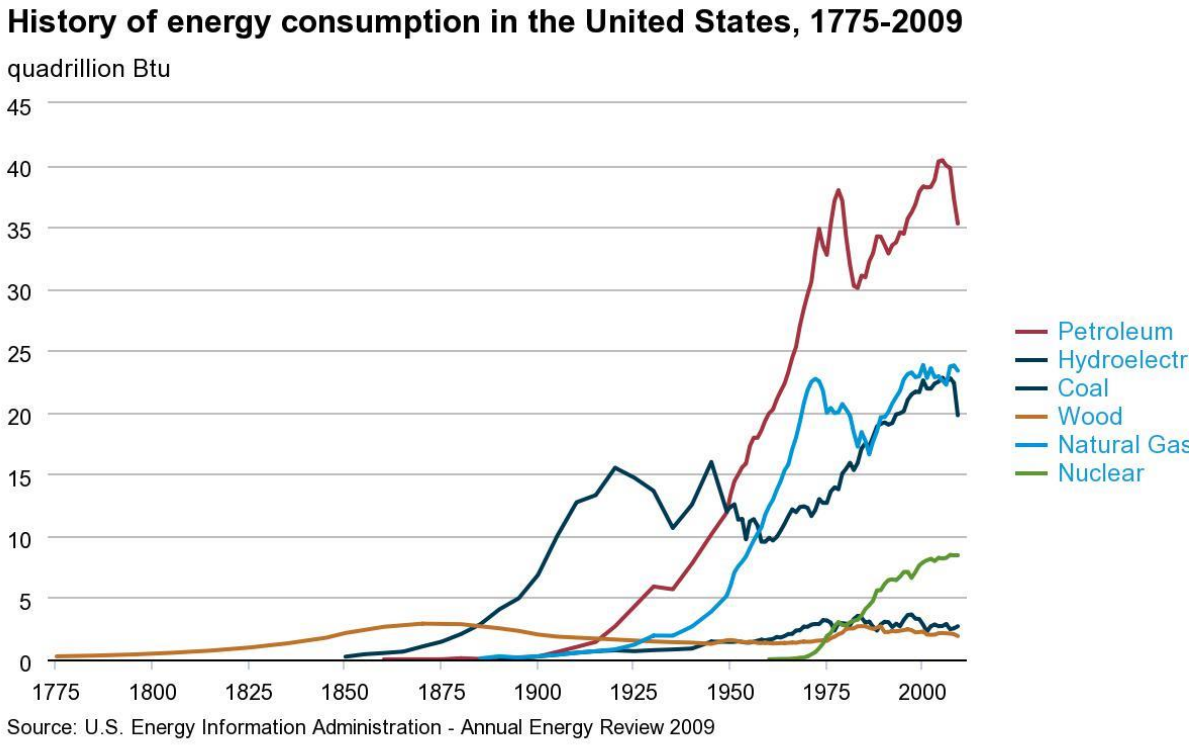

Figure 1. Total energy consumption in the United States from 1775-2009.[1]

The trend seen in both global and domestic energy consumption is a positive trend for economic growth and technological advancement. However, there are several problems correlated with our unprecedented energy consumption. The primary sources of energy that we utilize are fossil fuels, which are nonrenewable resources that have a limited quantity and require millions of years to replenish in the Earth's crust. Fossil fuels provide for a robust and growing capitalistic, global economy. These factors are contributing to the depletion of nonrenewable resources. In addition, the amount of these fuels is challenging to know. Ultimately, the supply of these resources will be depleted entirely. Over the past decade several studies have predicted that fossil fuel reserves will be diminished relatively shortly with depletion times of 35, 107, and 37 years for oil, coal and gas, respectively.[2]

The extinction of fossil fuels that provide for the majority of global energy needs would ruin the current global economy. The continual combustion of fossil fuels for energy usage releases carbon dioxide (CO_2) into the atmosphere. Carbon dioxide is a greenhouse gas, a gas that traps heat in the atmosphere, causing global temperatures to rise. The elevated levels of carbon dioxide pose a direct relationship with global temperature levels. Elevated greenhouse gases are a leading factor for the increase of 0.85 (±0.2) ^{o}C in global mean surface temperature (GMST) from 1880 to 2012.[3] Elevated temperatures will influence several negative consequences, such as the melting of ice caps resulting in a rise in global sea level. Sea levels have changed over time, depending on global temperature and glaciation. At several points in history, there have been consistent rises in the sea level followed by a rapid drop in the sea level. Most of these low sea level periods have coincided with mass extinctions of marine organisms.[10] Over time, sea levels and atmospheric gas levels have shown to rise and decline leading to these mass extinctions, yet the rate at which atmospheric carbon dioxide is currently rising is a profound concern. These issues associated with

high nonrenewable energy consumption levels need to be scrutinized and altered to provide a safe and sustainable future.

1.2: A solution to the rising energy demands

A plausible solution to address our rising energy consumption is to utilize renewable resources that both minimize the consumption of fossil fuels and reduce the negative effects imposed on the environment. Renewable energy is derived from sources that are not limited, like fossil fuels, and provide a limitless potential if unleashed. Hence, renewable resources are an attractive alternative solution given the minimal environmental effects, and sheer abundance of supply. Since the 1970s, there has been an increased focus on the area of renewable resources to supplement our growing energy concerns. In 2014, a study conducted by BP (British Petroleum) estimated that the global renewable energy share of energy consumption was approximately 9%, yet fossil fuels still accounted for 87% of energy consumption.[4] The major types of renewable energy sources are biomass, hydropower, geothermal, wind, and solar. The three primarily studied and implemented areas consist of hydropower, wind, and solar energy.

Hydropower energy is a renewable resource that taps into moving water sources, rivers, and lakes, while maximizing the force of water to produce mechanical energy. In the United States alone, hydroelectricity accounts for approximately 6.6% of total US utility-scale electricity generation.[5] Water sources are abundant throughout the world offering a level of feasibility that fossil fuels fail to permit. However, the source of hydroelectric power must be located on or near a water source to benefit from this field. Hence, this resource is limited in the availability of a moving water source capable of forcing water through a change in elevation to yield electricity, or energy. Another downside to hydroelectric power is the extraneous modification to the water source that negatively transforms the aquatic environment.[5] Hydroelectric energy sources have

maximized and will continue to meet some of our energy needs, yet fail to meet global demand alone.

Another renewable resource currently utilized is wind energy. Wind energy is of importance given the clean energy it provides without the combustion of fossil fuels that result in atmospheric carbon dioxide. Wind turbines can be constructed and installed on farms or ranches of the world to harness wind energy to create electricity in a cost-effective manner.[6] The majority of wind turbines are installed in rural areas, which requires the development of transmission lines to carry the electricity over a large distance to reach urban centers. Another disadvantage is the associated hazard and negative costs inflicted on local organisms, such as birds that fly into the apparatus.[6]

The other common renewable resource that can be utilized in a non-environmentally taxing method is solar energy. Solar energy is an attractive alternative to achieve energy without fossil fuels given its unmatched abundance and clean footprint on the Earth. Solar energy is the most superior renewable energy source based on availability, cost effectiveness, accessibility, and capacity. On a daily basis, the sun emits energy at the rate of 3.8×10^{23} kW, where 1.8×10^{14} kW is intercepted by the Earth.[7] In the United States alone, photovoltaic (PV) panels covering 0.6% of the total area could supply enough electricity to power the entire United States.[8] Solar energy has an advantage over wind and hydropower sources in that availability is not restricted to a specific location, thus location can be rural or urban. Solar energy harvesting mechanisms, such as solar panels, can be installed on top of buildings, or even the windows themselves permitting practically.[8] Another advantage of solar energy over wind or hydropower energy is the minimal consequences inflicted on the animal biosphere located in area. Solar energy offers unmatched potential if accessed appropriately and harvested in a cost-effective manner to provide the world

with an energy source that can generate the required electrical energy demands in an environmentally friendly manner.

1.3: Dye-Sensitized Solar Cells

Dye-sensitized solar cells (DSSCs) are photoelectrochemical solar devices that offer a plausible alternative to the current unstable consumption of fossil fuels for global energy necessities. DSSCs are attractive given their low cost, high light-to-electricity conversion efficiencies, and their minimized environmental footprint. A DSSC consists of four common components: a photoanode, a sensitizer dye, a cathode, and redox shuttle. The photoanode is a semiconducting porous metal oxide with high surface area, typically nanocrystalline titanium oxide (TiO_2). On the backside of the semiconducting metal oxide is a transparent conductive oxide (TCO), while the dye is absorbed onto the TiO_2 surface that is in contact with the redox shuttle solution. The redox shuttle serves to regenerate the ground state sensitizer completing the electrical circuit between sensitized TiO_2 and the counter electrode; the traditional redox shuttle consists of iodide/triiodide redox pair (I_3^-/I^-).[12] A general schematic of a dye-sensitized solar cell is shown in **Figure 2.**

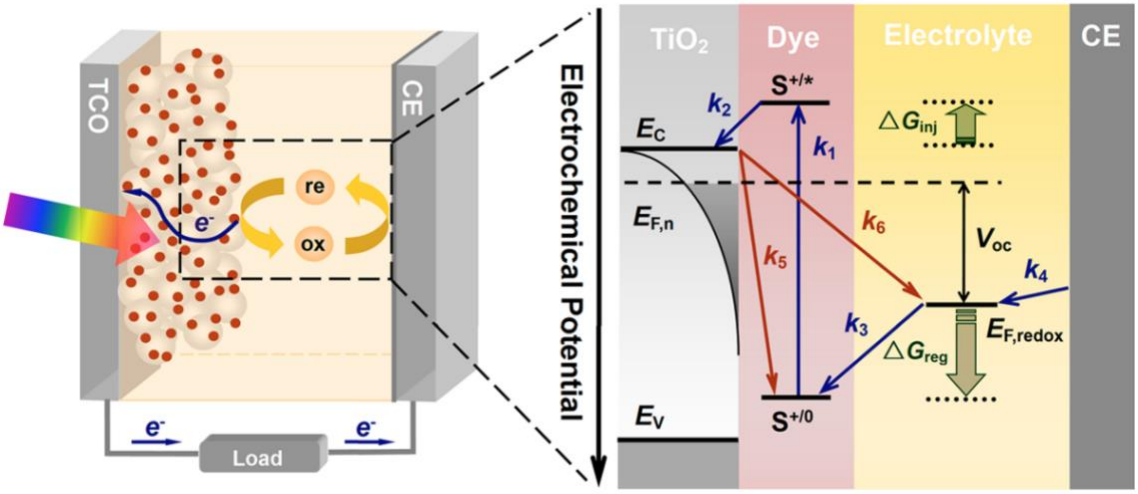

Figure 2. A general schematic for a DSSC.[20]

Development of a highly efficient DSSC requires an ideal sensitizer dye with a lowest unoccupied molecular orbital (LUMO) that has a more negative reduction potential than the semiconductor's conduction band and a highest occupied molecular orbital (HOMO) that has a more positive reduction potential than the redox couple.[20] The harnessing of sunlight for electrical power is a result of the excitation of the sensitizer within the DSSC. When incident light strikes the DSSC, the light will travel through the TCO layer reaching the photoanode with adsorbed dye resulting in the excitation of an electron. The excited electron is injected into the semiconducting porous metal oxide, and the oxidized dye is regenerated by the redox couple. The injected electron will flow through the semiconductor band to an external circuit reaching the counter electrode (CE) or cathode. Electron transfer at the cathode regenerates the oxidized redox shuttle to complete the circuit. However, unproductive back electron transfer, or recombination, of the injected electron with the oxidized sensitizers or with the oxidized form of the redox couple can also occur during this process. These two electron transfer reactions (shown by the red arrows in Figure 2) are undesirable as it reduces the efficiency of the DSSC.[20]

1.4: Recent shift to Transition Metal Redox Shuttles

One of the most efficient redox mediators employed thus far has been I_3^-/I^-, due to the fact that I^- allows for fast regeneration of the oxidized dye while minimizing recombination losses.[9] However, this redox mediator is a two-electron system. The first step involves electron transfer from I^- to regenerate the reduced form of the redox shuttle forming the radical, $I_2^{\bullet -}$. Hence, the second step must regenerate I^- and I_3^- for continued electron transfer.[25] The formation of this intermediate step is energetically unfavorable compared to a one-electron redox systems. This has given rise to alternative one-electron redox couples for DSSCs.

Recent studies have investigated the use of metal organic redox mediators in place of the I_3^-/I^- redox couple. A prominent advantage to these systems is their adjustable molecular ligands for fine-tuning the redox potential. Thus, these one-electron redox shuttles must be designed to pair appropriately with the LUMO and HOMO levels of the sensitizer dye.[20] The tunability and variation of these redox shuttles has been heavily researched over the past couple of decades, resulting in several examples of more efficient redox systems for DSSCs.

1.5: Previous Studies of Redox Shuttles

Redox shuttles play a critical role in completing the circuit by transferring an electron collected at the counter electrode to the oxidized dye at the photoanode in dye-sensitized solar cells. Several transition metal-based redox shuttles have been implemented for this role such as $[Co(bpy)_3]^{3+/2+}$, which has yielded power conversion efficiencies as high as 13%.[15] Poly(pyrazolyl)borate complexes were first studied by Trofimenko and extensive investigations on the unsubstituted and the 3,5-dimethyl ligand have occurred from 1971-1993.[18,21] Some twenty-five years later, poly(pyrazolyl)borate compounds have been investigated as alternative redox shuttles in quantum dot-sensitized solar cells (QDSSCs). These Mn poly(pyrazolyl)borates displayed lower recombination at the TiO_2 than the most efficient redox shuttle, $[Co(bpy)_3]^{3+/2+}$.[20] The $[Mn(Tp)_2]^{1+/0}$ redox mediator used in this study in shown in **Figure 3**. Consequently, the downfall of these poly(pyrazolyl)borate redox mediators revolved around their low solubility which limited the sustained photocurrent that was possible. A previous study investigated the electrochemical properties of iron(II)-bis[tris(pyrazolyl)methane] in CH_3CN, which exhibited a chemically reversible oxidation at 0.69 V vs. $Fc^{+/0}$.[19] However, this study did not examine this complex as a redox shuttle in a DSSC.

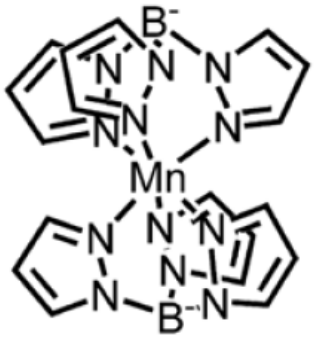

Figure 3. Manganese tris(pyrazolyl)borate redox shuttle complex investigated by Morris *et al*.[12]

1.6: The Rationale of this Study

Poly(pyrazolyl)borate ligands have been studied extensively over the past four decades following Trofimenko's initial publication on this class of compounds.[21] These ligands have been utilized as an exceptional chelating agent for first-row transition metals. The coordinating ability of the poly(pyrazolyl)borate ion is a consequence of favorable electronic and geometric factors.[21] The tris(pyrazolyl)borate ion is highly tunable and can be prepared with a wide range of different R groups at different positions as shown in **Figure 4.**[15] Tris(pyrazolyl)borate ligands have been employed in numerous capacities, including oxidative alkane C-H bond functionalization[16] and metalloenzyme model complexes.[17] These anionic tridentate ligands have C_{3v} symmetry and bind metal ions in a *facial* orientation, often enforcing octahedral geometries with notable exceptions involving derivatives with bulky substituents at the 3-position of each donor. Many studies have focused on substitutions at the 3- and 5-positions of each pyrazole ring with various R groups such as alkyl, aryl, and halide groups as well as fused rings.[18] However, relatively few investigations have been reported involving the effects of substituents at the 4-position of the pyrazole donors. Trofimenko concluded that the 4-position of the Tp ligand can be fine-tuned, as the 4-position of the pyrazole is remote from the metal; however, added substituents can be used to increase or

decrease the overall electron density of the ligand via their electron-donating or -withdrawing properties, respectively.[18]

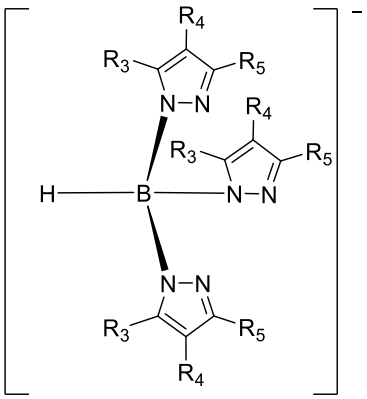

Figure 4. Structure of tris(pyrazolyl)borate (Tp) with variable R groups at the 3-, 4-, and 5-positions.[15]

Morris and coworkers recently employed manganese bis[hydrotris(pyrazolyl)borate] as a redox shuttle, utilizing the Mn(III/II) couple, in QDSSCs.[12] However, high photocurrent was not sustainable due in large part to the poor solubility of the compound, presumably the neutral Mn(II) species in particular, which limits mass transport. Mn(III)/(II) poly(pyrazolyl)borates have been examined due to their kinetic barrier from a high-to-low spin transition resulting in a lower heterogeneous electron transfer rate that reduces recombination.[20] Poly(pyrazolyl)borate complexes have more positive reduction potentials than $[Co(bpy)_3]^{3+/2+}$ establishing the viability of Mn poly(pyrazolyl)borates as promising redox mediators with higher solubilities. In this context, we sought to develop new redox shuttles based on tris(pyrazolyl)borate compounds for dye-sensitized solar cells. We reasoned that adding alkyl substituents to the pyrazole donors would enhance solubility in organic solvents such as acetonitrile. Herein we report first-row transition metal compounds of manganese(II), iron(II), cobalt(II), and nickel(II) of bishydrotris(3,5-dimethyl-4-ethylpyrazolyl)borate. These compounds were characterized and compared to

analogous compounds supported by unsubstituted tris(pyrazolyl)borate as well as those of the less substituted tris(3,5-dimethylpyrazolyl) borate to quantify the impact on properties such as redox potentials and solubility upon substitution at the 4 position.

Schultz and coworkers recently determined coupled electron-transfer and spin-exchange reactions of metal-bis[tris(pyrazolyl)methane] complexes.[19] They reported similarities in the electrochemical, magnetic, and spectroscopic properties of these Tpm complexes in comparison to the corresponding Tp complexes with the only major difference being that the M(III/II) potential difference of ~1 V more positive for $[M(Tpm)_2]^{3+/2+}$ derivatives than for the $[M(Tp)_2]^{1+/0}$ couples due, in large part, to the net charge differences. A key discovery in this study is the integrity of $[Fe(Tpm)_2]^{2+}$ complex is maintained in acetonitrile, while this complex undergoes ligand dissociation in DMF.[19] This property is of necessary concern for the application of this redox shuttle in DSSCs. The tridentate ligand for the iron complex synthesized in this study is shown in **Figure 5**. Given the electrochemically reversible redox couple, increases in the reduction potential, and the solubility in acetonitrile, we predict that we can produce an efficient redox mediator using this ligand framework.

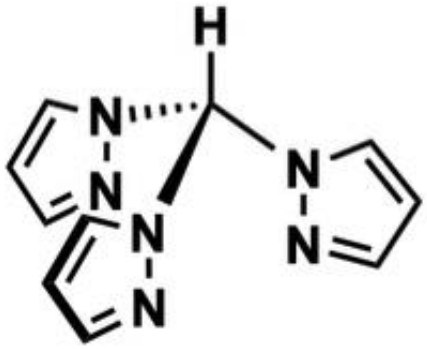

Figure 5. Structure of tris(pyrazolyl)methane (tpm), the neutral tridentate ligand coordinated to the iron complex synthesized in this study.

2. Experimental Procedures

2.1: Materials and Methods

Unless otherwise noted, all synthetic manipulations were performed under nitrogen atmosphere utilizing standard Schlenk techniques or in an MBraun glovebox. Dichloromethane, and tetrahydrofuran were dried with a Pure Process Technology solvent purification system. Compounds iodoethane, potassium borohydride, and iron (II) chloride tetrahydrate were purchased from Sigma Aldrich. Anhydrous metal salts nickel (II) chloride hexahydrate and cobalt (II) chloride hexahydrate, were purchased from VWR Life Science and Beantown Chemical, respectively. The acetylacetonate precursor 2,4-pentanedione was purchased from Alfa Aesar. All other chemicals were reagent or ACS grade, purchased from commercial vendors, and used without further purification. ^{1}H NMR spectra were obtained with using a Bruker 300 spectrometer operating at 300MHz. Spectra were calibrated to residual protiated solvent peaks; chemical shifts are reported in ppm. High Resolution Electrospray ionization mass spectrometry (ESI-MS) spectra were obtained with a Waters SYNAPT HDMS Q-TOF mass spectrometer. IR spectra were obtained on an Agilent Technologies Cary 600 series FTIR spectrometer as a KBR pellet. UV-visible spectra were recorded on an Agilent/Hewlett-Packard 8453 UV-Visible Spectrophotometer with diode-array detector.

2.2: Synthetic Route for tris(pyrazolyl)borate ligand

The overall synthetic route for the tridentate ligand used in this study, tris(3,5-dimethyl-4-ethylpyrazolyl) borate **($Tp^{Me_2 4Et}$)**, is shown in **Figure 6.**

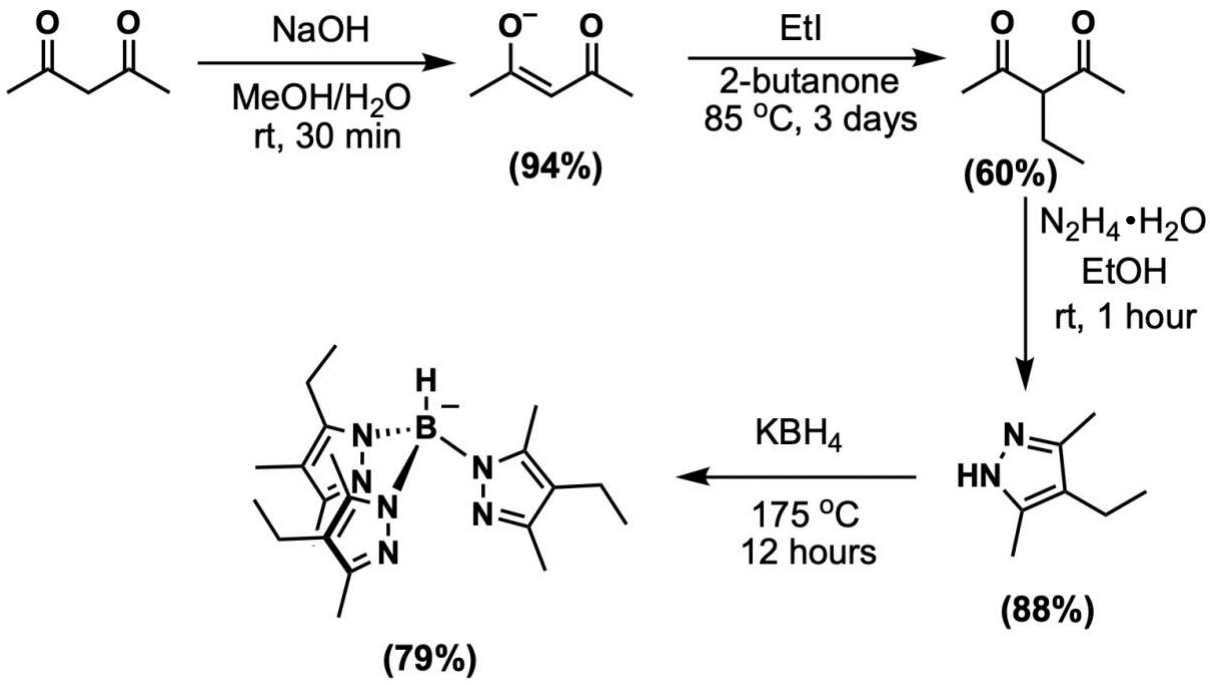

Figure 6. Synthetic route for **($Tp^{Me_2 4Et}$)**.

2.3: Synthesis of Tp ligand

Sodium Acetylacetonate (1)

To generate the first ligand precursor, Acetylacetone (30.9 mL, 0.3 mol) was slowly added dropwise to a solution of NaOH (8 g, 0.2 mol) in methanol/water (4:1; 50 mL). During the whole process, the mixture was stirred at room temperature so that the temperature of the reaction system remained constant. Once the reaction was finished, the products were washed three times with ice-cooled methanol after filtration in vacuum and then placed in a vacuum drying oven to give the product as a white solid (19.2 g) in 94% yield.

3-Ethylpentane-2,4-dione (2)

The sodium pentane-2,4-dione (3.2 g, 26.0 mmol) was then mixed with ethyl iodide (66.6 mL, 832 mmol) and 2-butanone (12 mL) in a pressure vessel and heated at 80-85^{o}C for 3 days under vacuum. Water (120 mL) and toluene (160 mL) was added to the mixture and the colored toluene layer was separated. The toluene and excess ethyl iodide were removed in vacuo. Crude Yield: 2.01 g (60%).

3,5-dimethyl-4-ethylpyrazole (3)

Hydrazine monohydrate (7.3 g, 0.146 mol) was added dropwise to a solution of 3-ethyl-2,4-pentanedione (18.71 g, 0.146 mol) in ethanol (100 mL). This reaction was mildly exothermic and stirred vigorously for one hour. Removal of solvent under vacuum yielded a yellow crystalline product. Yield: 15.68 g (88%). **^{1}H NMR (CD_2Cl_2):** δ 10.16 (NH, s, 1H), 2.21 (3,5-CH_3, t, 6H), 2.37 (-CH_2Me, q, 2H), 1.06 (CH_2CH_3, t, 3H).

Potassium tris(3,5-dimethyl-4-ethylpyrazolyl) borate (4)

3,5-dimethyl-4-ethylpyrazole (4 g, 32.2 mmol) and KBH_4 (0.288 g, 5.34 mmol) were placed in a 50 mL round-bottomed flask under nitrogen. The temperature was steadily increased to 175 ^{o}C and maintained overnight while stirred, after which time hydrogen evolution had ceased. Majority of the excess pyrazole was distilled off by attaching a short path distillation the round bottom flask. The final traces of pyrazole were removed by sublimation onto a dry ice/acetone probe under vacuum to leave pure potassium tris(3,5-dimethyl-4-ethylpyrazolyl)borate. Yield: 1.8 g (79%). **IR (KBr)** 2239 cm^{-1} (B-H). **^{1}H NMR (d_6-acetone):** δ 2.37 (q, 6H, CH_2CH_3), 2.19 (s, 9H, CH_3), 2.19 (s, 9H, CH_3), 1.06 (t, 9H, CH_2CH_3).

2.4: Synthesis of transition metal tris(pyrazolyl)borate complexes

Nickel(II) bishydrotris(3,5-dimethyl-4-ethylpyrazolyl) borate

A mixture of potassium tris(3,5-dimethyl-4-ethylpyrazolyl) borate (0.1 g, 0.237 mmol) and $NiCl_2 \bullet 6H_2O$ (0.0286 g, 0.119 mmol) were placed in a 50 mL round-bottomed flask in methanol (7.5 mL) under nitrogen. This reaction stirred overnight at room temperature. The mixture was evaporated to dryness in vacuo. Yield 0.048 g (83%). The product was confirmed with HR-MS. **IR (KBr)** 2508 cm^{-1} (B-H).

Cobalt(II) bishydrotris(3,5-dimethyl-4-ethylpyrazolyl) borate

A mixture of potassium tris(3,5-dimethyl-4-ethylpyrazolyl) borate (0.1 g, 0.237 mmol) and $CoCl_2 \bullet 6H_2O$ (0.0282 g, 0.119 mmol) were placed in a 50 mL round-bottomed flask in methanol (7.5 mL) under nitrogen. This reaction stirred overnight at room temperature. The mixture was evaporated to dryness in vacuo. Yield 0.048 g (84%). The product was confirmed with HR-MS. **IR (KBr)** 2507 cm^{-1} (B-H).

Iron(II) bishydrotris(3,5-dimethyl-4-ethylpyrazolyl) borate

A mixture of potassium tris(3,5-dimethyl-4-ethylpyrazolyl)borate (0.1 g, 0.237 mmol) and $FeCl_2 \bullet 4H_2O$ (0.0236 g. 0.119 mmol) were placed in a 50 mL round-bottomed flask in methanol (7.5 mL) under nitrogen. This reaction stirred overnight at room temperature. The mixture was evaporated to dryness in vacuo. Yield 0.0457 g (80%). The product was confirmed with HR-MS. **IR (KBr)** 2512 cm^{-1} (B-H).

Manganese(II) bishydrotris(3,5-dimethyl-4-ethylpyrazolyl) borate

A mixture of potassium tris(3,5-dimethyl-4-ethylpyrazolyl)borate (0.1 g, 0.237 mmol) and $MnCl_2$ (0.0149 g. 0.119 mmol) were placed in a 50 mL round-bottomed flask in methanol (7.5 mL) under nitrogen. This reaction stirred overnight at room temperature. The mixture was evaporated to dryness in vacuo. Yield 0.0439 g (77%). The product was confirmed with HR-MS.

2.5: Synthetic Route for tris(pyrazolyl)methane ligand

The overall synthetic route for the second tridentate ligand used in this study, tris(pyrazolyl) methane (Tpm), is shown in **Figure 7**.

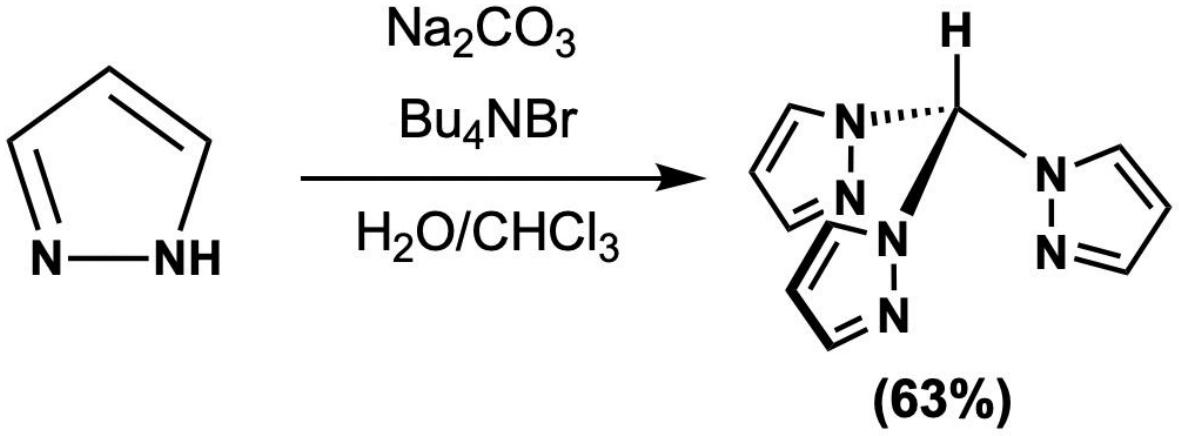

Figure 7. Synthetic route for Tpm.

2.6 Synthesis of Tpm

Tris(1-pyrazoyl)methane

Distilled water (73.5 mL) was added to a 250 mL round bottom flask containing a mixture of pyrazole (4.0 g, 73.5 mmol) and tetra-n-butylammonium bromide (1.175 g, 3.675 mmol). With vigorous stirring, sodium carbonate (46.75 g, 0.45 mol) was added gradually to the reaction mixture; constant stirring increases the efficiency of the reaction1. After cooling to near room

temperature, chloroform (36.75 mL) was added and the flask was equipped with a reflux condenser. This mixture was heated at gentle reflux for 3 days over which time it became a pale-yellow emulsion. The mixture was allowed to cool to r.t. and filtered through a Buchner funnel to remove the excess base. To the filtrate was added diethyl ether (125 mL) and H_2O (75 mL). The organic layer was separated and the aqueous layer extracted with diethyl ether (200 mL). The combined organic layers were then washed with saturated brine solution (50 mL). The organic layer was treated with decolorizing charcoal and dried over sodium sulfate. The mixture was filtered and the solvent removed by rotary evaporation. The resulting pale-yellow solid (3.15 g, 63%) was then dried under vacuum. **^{1}H-NMR (acetone-d$_6$):** δ 8.73 (s, 1H, HC), 7.86 (d, 3H, 3-H (pz)), 7.62 (d, 3H, 5-H (pz)), 6.40 (d of d, 3-H, 4-H (pz)).

2.7: Synthesis of [Fe(tpm)$_2$]$^{2+/3+}$

The synthesis of the iron(II) complex was accomplished by stirring tris(1-pyrazoyl)methane, (0.250 g, 1.167 mmol) and iron(II) chloride (0.0739 g, 0.584 mmol) in methanol (20 mL). The mixture was stirred overnight at room temperature under nitrogen atmosphere resulting in a red-violet precipitate. The precipitate was dried under vacuum, then dissolved in anhydrous acetonitrile and crystallized with slow diffusion diethyl ether crystallization at room temperature yielding microcrystalline violet-red crystals. Yield: 0.223 g (79%). The product was confirmed with HR-MS. The cyclic voltammetry data matched the spectra reported in literature.[19]

3. Results and Discussion

3.1: Synthesis of Tp Ligand

Synthesis of the tridentate ligand was accomplished in four steps. In summary, a β-diketone was reacted with sodium hydroxide to yield an electrophilic complex for alkylation. The alkylating agent, ethyl iodide, will be able to act as a nucleophile to alkylate the β-diketone at the 4-position. After successful alkylation, the β-diketone reacts with hydrazine to form the substituted 3,5-dimethyl-4-ethylpyrazole. This reaction first forms an acid catalyzed imine on one of the carbonyl groups, followed by a second attack on the other carbonyl group to form a second imine group. This diamine compound gets deprotonated to yield the final substituted pyrazole. The final step consists of reacting the pyrazole with potassium borohydride giving the alkylated Tp ligand.

Production of the ligand gave reasonable yields ranging from 60 to 94%. Throughout the synthesis, there were NMR instrumentation utilized to ensure proper products were being synthesized from the previous precursor. The NMR data for these steps is shown in the **Supporting Information.**

3.2: Synthesis of Transition Metal Tp Complexes

Furthermore, the synthesized ligand can now react with first-row transition metals to achieve the final desired complex under study. The ligand was stirred in a solution containing degassed methanol with a hydrated metal chloride. To ensure complete metalation to the Tp ligand, the reaction was carried out overnight at room temperature. Due to the possibility of oxidizing the M^{2+} to the M^{3+}, all reactions were carried out under a nitrogen atmosphere. Complete characterization of the complexes was achieved – high-resolution mass spectrometry (HRMS),

Fourier Transform-Infrared (FT-IR) spectroscopy, UV-Visible spectroscopy, cyclic voltammetry (CV), and solubility properties.

3.3: Characterization of Transition Metal Tp Complexes

The first-row transition metals under study were manganese, iron, cobalt, and nickel. The last three of which were characterized completely. Synthesis of these complexes were confirmed with HR-MS. Further analysis was done with FT-IR highlighting the shift in the borohydride (B-H) bond found within all the complexes. FT-IR for these complexes is shown in **Figures 8, 9,** and **10** for the Fe, Co, and Ni complexes, respectively. Borohydride shifts were found to be 2512, 2507, and 2508 cm^{-1} for Fe, Co, and Ni complexes, respectively. These values are consistent with known literature values of these transition metals with the unsubstituted Tp and 3,5-dimethyl-Tp complexes as shown in **Table 3**.[11]

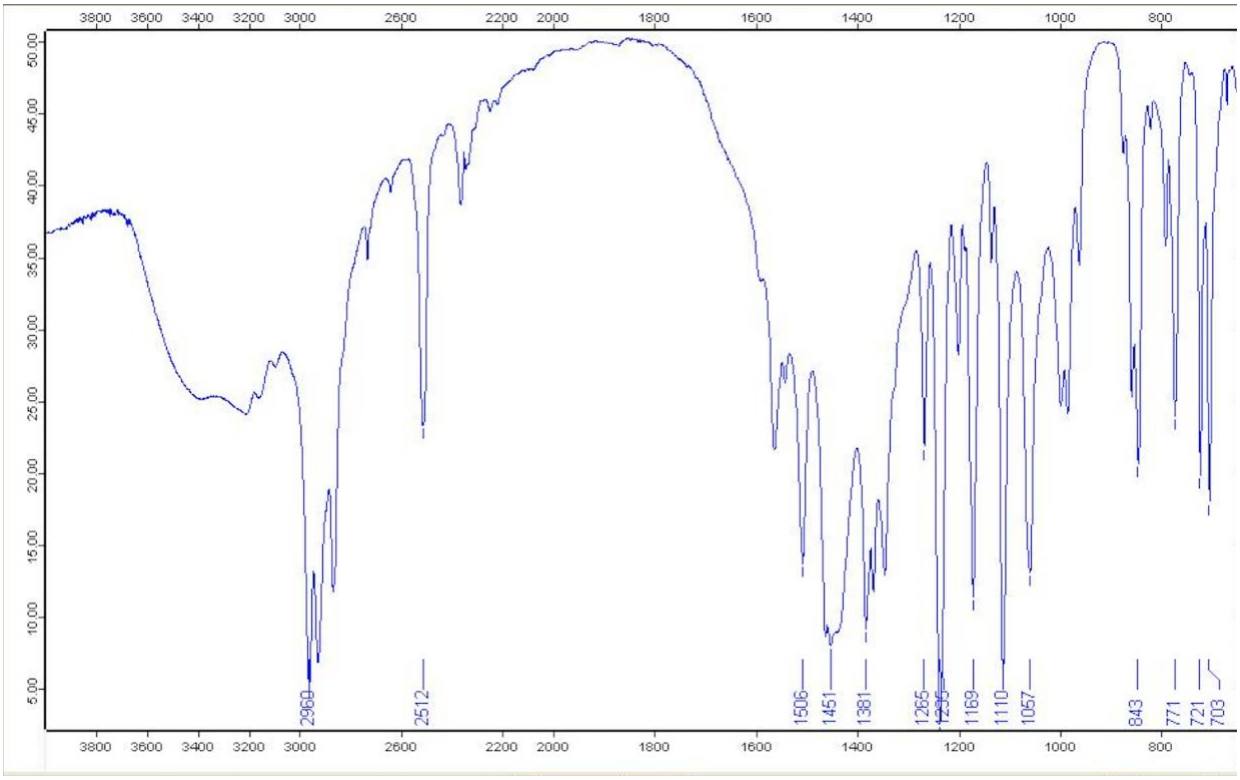

Figure 8. FT-IR of Fe(II) $(Tp^{Me_2 4Et})_2$.

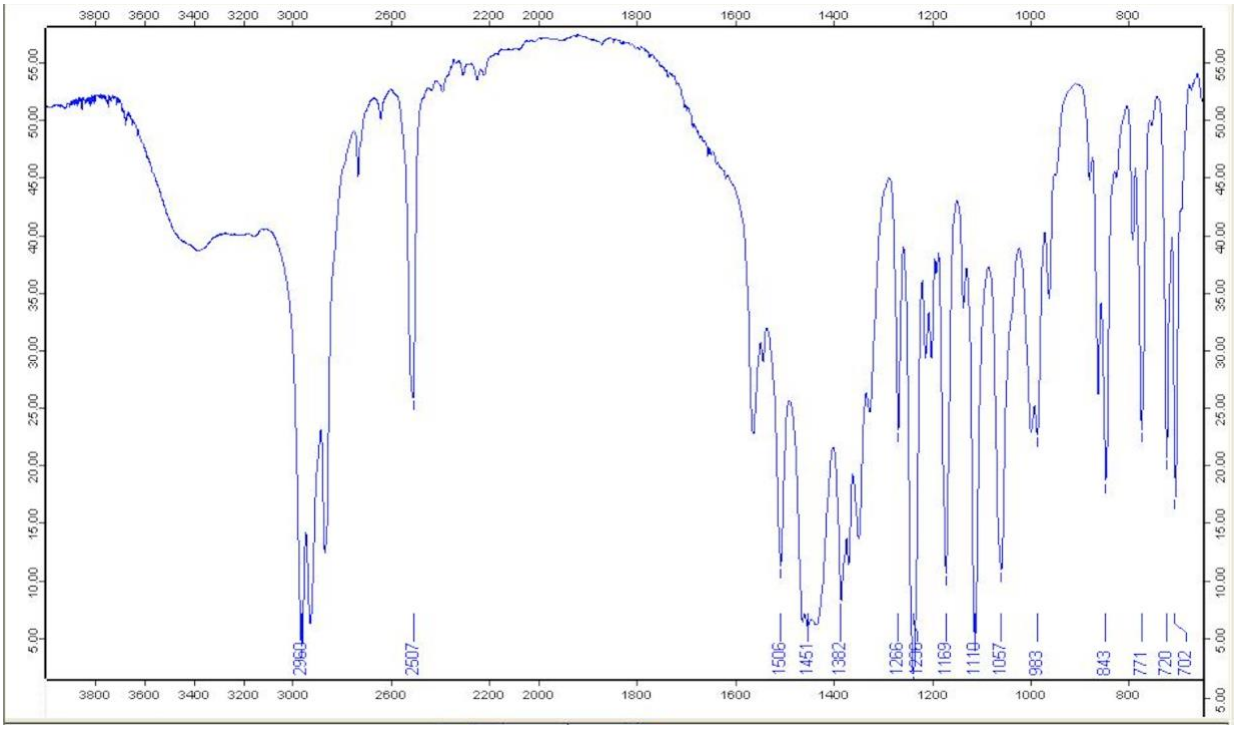

Figure 9. FT-IR of Co(II) $(Tp^{Me_2 4Et})_2$.

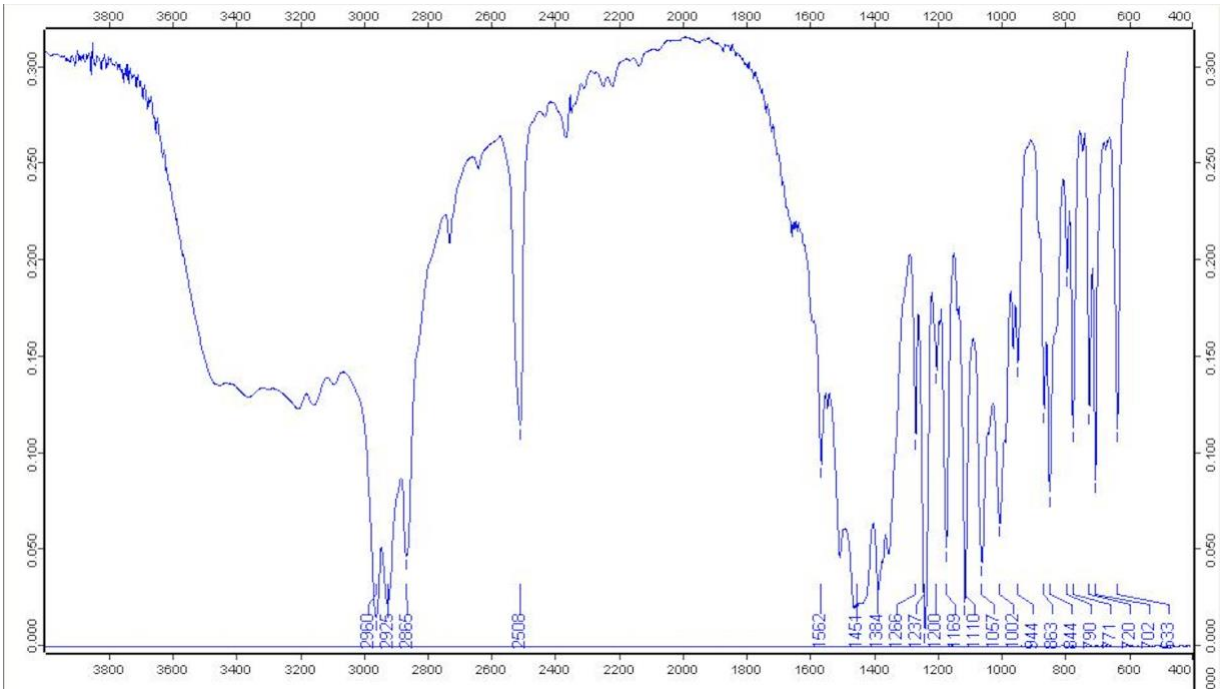

Figure 10. FT-IR of Ni(II) $(Tp^{Me_2 4Et})_2$.

	IR [cm^{-1}] ν(B-H)	Ref.
$Fe(Tp)_2$	2485	[11]
$Co(Tp)_2$	2464	[11]
$Ni(Tp)_2$	2467	[11]
$Fe(Tp^*)_2$	2508	[11]
$Co(Tp^*)_2$	2506	[11]
$Ni(Tp^*)_2$	2508	[11]
$Fe(Tp^{Me_2 4Et})_2$	2512	this work
$Co(Tp^{Me_2 4Et})_2$	2507	this work
$Ni(Tp^{Me_2 4Et})_2$	2508	this work

Table 2. FTIR Data from Metal-Bis[tris(pyrazolyl)borate] complexes. Tp = tris(pyrazolyl)borate,[11] Tp* = tris(3,5-dimethylpyrazolyl)borate,[11] and $Tp^{Me_2 4Et}$ = tris(3,5-dimethyl-4-ethylpyrazolyl)borate.

Another characterization technique utilized was Ultraviolet-Visible spectroscopy which can give quantitative analysis using Beer's Law. UV-Vis spectra for these complexes is shown in **Figures 11, 12,** and **13** for the Fe, Co, and Ni complexes, respectively. These UV-Vis peaks are shown in comparison to other first-row transition metal Tp complexes in **Table 3.** The iron complex was consistent with the literature, yet the other complex peaks shifted or were not present.[26]

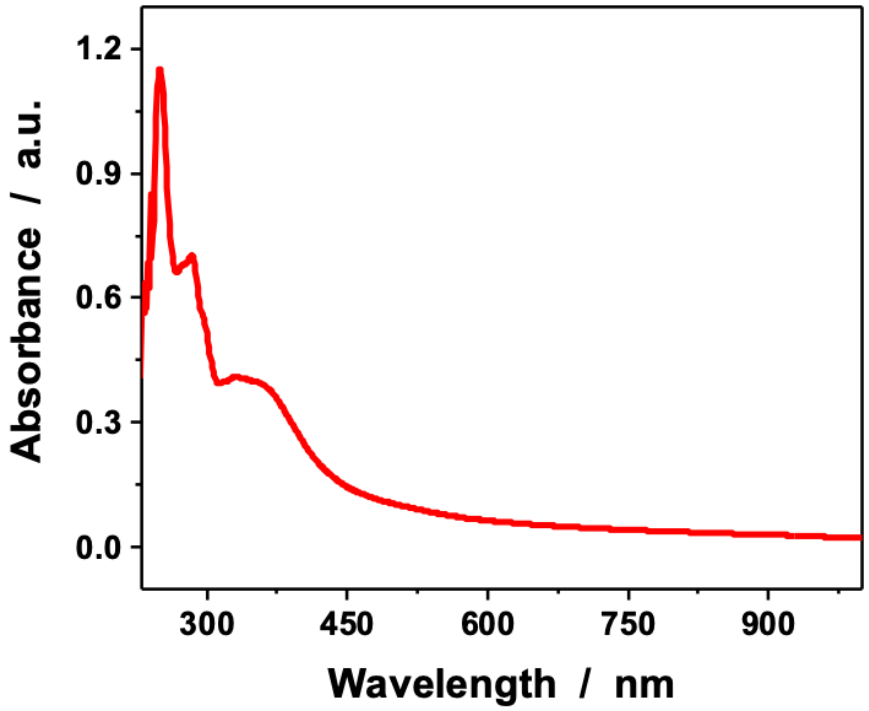

Figure 11. UV-Vis spectra for $Fe_{(II)}$ $(Tp^{Me_2 4Et})_2$.

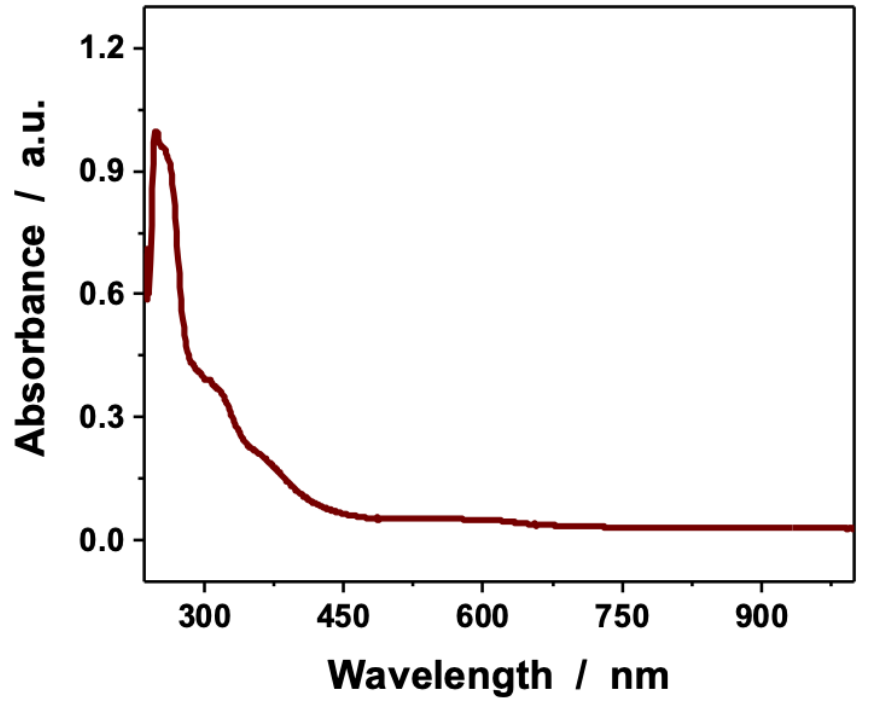

Figure 12. UV-Vis spectra for $Co_{(II)}$ $(Tp^{Me_2 4Et})_2$.

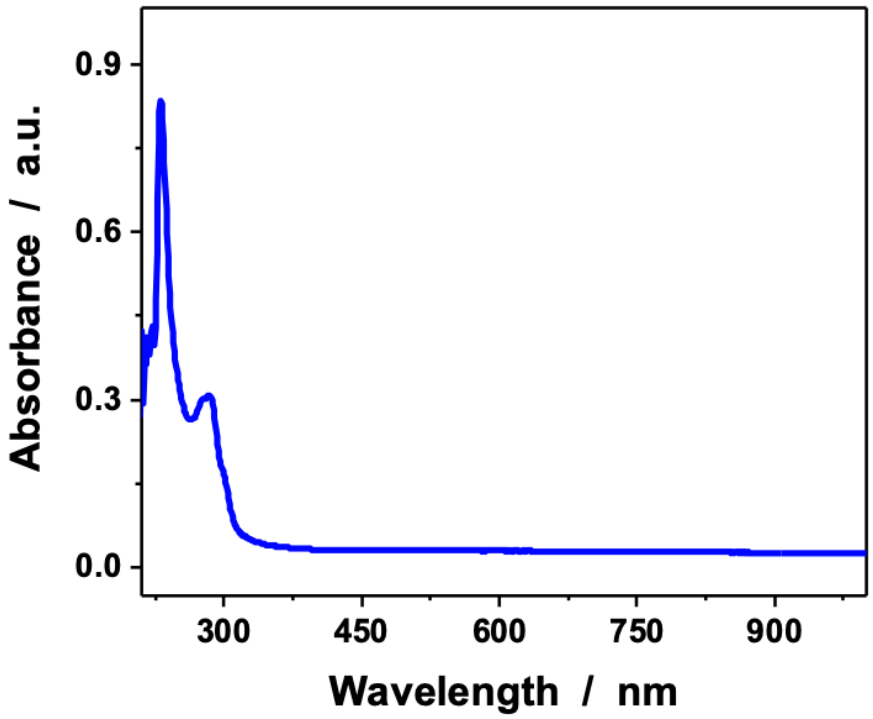

Figure 13. UV-Vis spectra for $Ni_{(II)}$ $(Tp^{Me_24Et})_2$.

	λ [nm]	Ref.
$Fe(Tp)_2$	226; 282; 316; 334	[26]
$Co(Tp)_2$	459; 515; 641; 901	[27]
$Ni(Tp)_2$	334;450;522;570;760;849	[27]
$Fe(Tp^*)_2$	230	[26]
$Co(Tp^*)_2$	--	--
$Ni(Tp^*)_2$	--	--
$Fe(Tp^{Me_24Et})_2$	222; 252; 288; 331	this work
$Co(Tp^{Me_24Et})_2$	250; 311	this work
$Ni(Tp^{Me_24Et})_2$	234; 287	this work

Table 3. UV-visible spectral data from Metal-Bis[tris(pyrazolyl)borate] complexes. Tp = tris(pyrazolyl)borate, Tp* = tris(3,5-dimethylpyrazolyl) borate, and Tp^{Me_24Et} = tris(3,5-dimethyl-4-ethylpyrazolyl) borate.

Ultimately, cyclic voltammetry is of key concern for redox shuttles as the potential must operate within certain parameters for use as a redox shuttle in DSSCs. Cyclic voltammetry works by cycling the potential of a working electrode and measuring the resulting current. For an inorganic complex to function as a redox shuttle in DSSCs, there must be a reversible oxidization between the M^{2+} and M^{3+}. Cyclic voltammetry was performed with a typical three-electrode setup using a CH Instruments 600E Series Potentiostat. The electrochemical cell was equipped with a glassy carbon disk working electrode, a platinum wire counter electrode, and a silver wire quasi-reference electrode. Dichloromethane (DCM) solutions containing 0.1 M Bu_4NPF_6 as the supporting electrolyte were used in the metal Tp complex studies. The CVs for the Fe, Co, and Ni complexes are shown in **Figure 14, 15,** and **16**, respectively. The redox couples are summarized in **Table 4.**

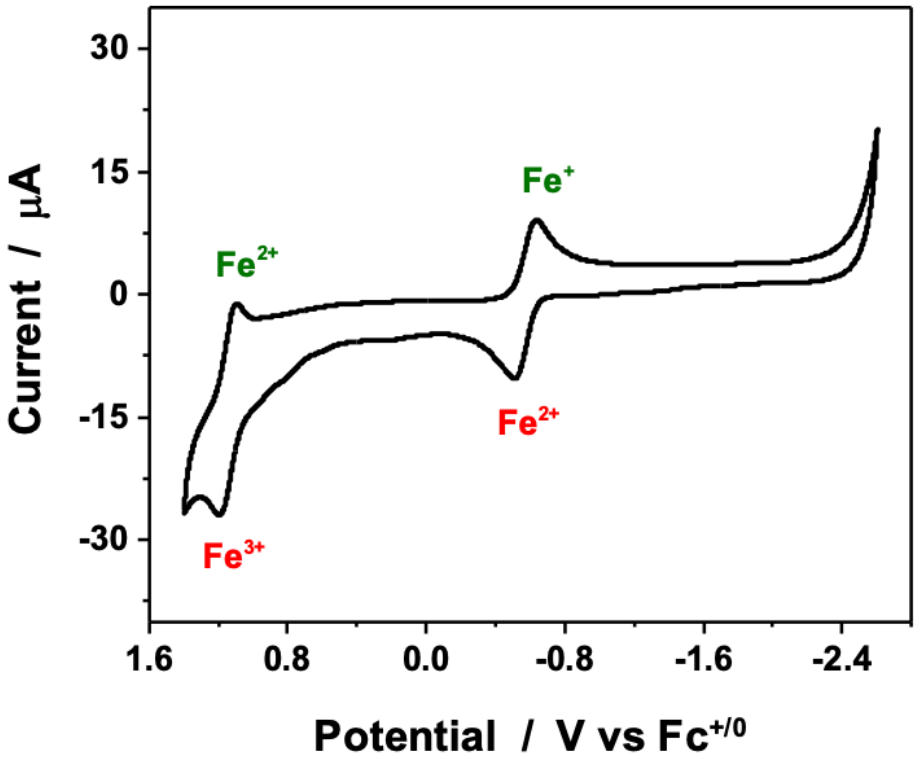

Figure 14. Cyclic voltammetry of a 1 mM solution of $Fe_{(II)}$ $(Tp^{Me_2 4Et})_2$ and 0.1M $TBAPF_6$ as a supporting electrolyte in dry DCM at 100 mV/s. Potential was referenced against ferrocene ($Fc^{+/0}$).

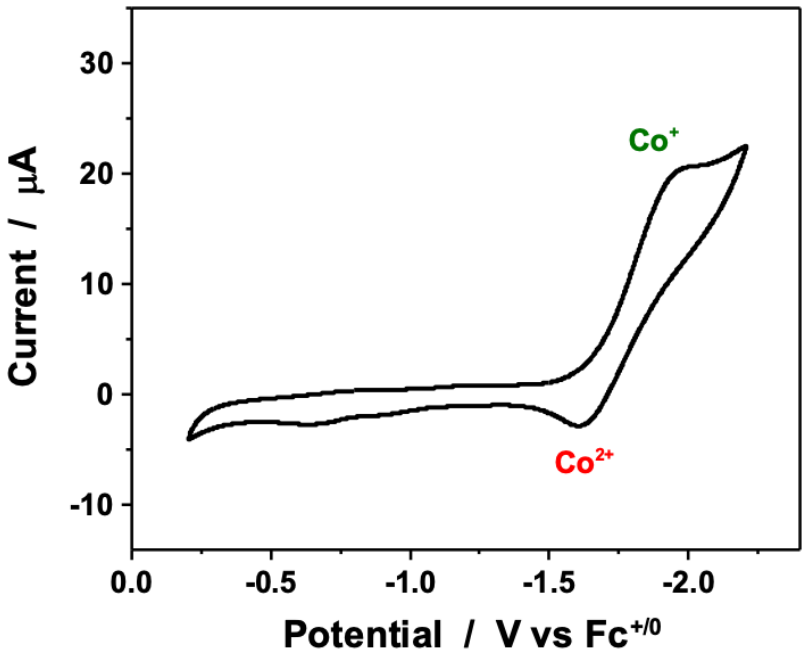

Figure 15. Cyclic voltammetry of a 1 mM solution of $Co_{(II)}$ $(Tp^{Me_2 4Et})_2$ and 0.1M $TBAPF_6$ as a supporting electrolyte in dry DCM at 100 mV/s. Potential was referenced against ferrocene ($Fc^{+/0}$).

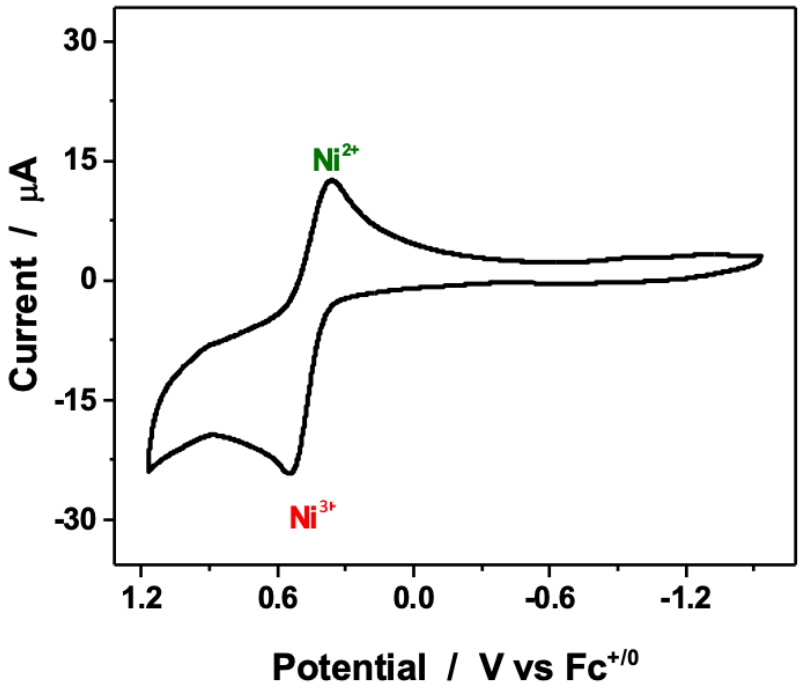

Figure 16. Cyclic voltammetry of a 1 mM solution of $Ni_{(II)}$ $(Tp^{Me_2 4Et})_2$ and 0.1M $TBAPF_6$ as a supporting electrolyte in dry DCM at 100 mV/s. Potential was referenced against ferrocene ($Fc^{+/0}$).

Redox Couple	$E_{1/2}$ (V vs $Fc^{+/0}$)
$Fe^{2+/+}$	-0.56
$Fe^{3+/2+}$	1.16
$Co^{2+/+}$	-1.73
$Ni^{3+/2+}$	0.48

Table 4. Electrochemical data for Metal-Bis[tris(3,5-dimethyl-4-ethylpyazolyl)borate] Redox Couples.

Lastly, another parameter required for DSSC redox shuttle is a solubility of 0.25mM in organic polar solvents, such as acetonitrile. Therefore, this study was able to quantify the solubility of Ni(II) $(Tp^{Me24Et})_2$ complexes for applicable use in DSSCs. Transition metal tris(pyrazolyl)borate complexes have little to no information regarding their max solubilities in organic solvents. Hence, this study was able to quantify the max solubilities in solvents, such as toluene, dichloromethane, tetrahydrofuran, and acetonitrile. The solubility found in hexanes and acetonitrile, two complexes on opposite ends of the polarity index provide little to no solubility. However, in solvents with a moderate polarity index of 2.4-4.0 yield substantially higher solubilities comparatively. Accurate molar solubilities were determined analytically by generating a saturated solution of each complex in anhydrous dichloromethane. The saturated solution was passed through a filter to remove any undissolved complex and weighed before evaporating the solution to dryness to determine the amount of each complex. The weights of each component were then used to determine the molarity of each saturation solution. The maximum solubilities associated with saturated solutions at room temperature for the studied tris(pyrazolyl)borate complexes are summarized in **Table 5** below. The

solubilities of these transition metal Tp complexes with varying substituents are sparingly soluble in organic solvents with solubilities ranging from 5.6 mM to 15.9 mM, far below the necessary solubility for DSSCs.

Complex	Solubility in DCM
$Ni(Tp)_2$	0.0159 M
$Ni(Tp^*)_2$	0.0095 M
$Ni(Tp^{Me_2 4Et})_2$	0.0056 M

Table 5. Solubility data for Nickel Tp complexes in anhydrous dichloromethane (DCM). Tp = tris(pyrazolyl)borate, Tp* = tris(3,5-dimethylpyrazolyl) borate, and $Tp^{Me_2 4Et}$ = tris(3,5-dimethyl-4-ethylpyrazolyl) borate.

The majority of transition metal redox shuttles in DSSCs have neutral ligands like 2,2'-bipyridine, as seen in $[Co(bpy)_3]^{3+/2+}$. Hence the overall charge is 2+ providing higher solubility in organic solvents such as acetonitrile. While the Tp ligand is anionic resulting in an overall neutral complex with lower solubility in common DSSC solvents. Additional ethyl and methyl groups on the tunable Tp ligand does not increase the solubility as hypothesized. This was experimentally shown that more alkyl chains on the Tp ligand result in lower solubilities as summarized in **Table 5**. Since the solubility of Tp complexes does not increase with alkylations, we transitioned to the study of tris(pyrazolyl)methane (Tpm) as a viable neutral ligand for redox shuttles with desired solubilities. Tpm is similar to Tp, as it is a tridentate *facial* ligand with the exception of a C-H bridgehead rather than a B-H bridgehead. The remainder of the study focuses

on the same first-row transition metals for use as redox shuttles in DSSC with the unsubstituted Tpm ligand.

3.4: Synthesis of Tpm Ligand

The synthesis of the tridentate ligand was accomplished in an effective manner. In summary, pyrazole was reacted with tetra-*n*-butylammonium bromide and sodium carbonate in 2:1 water/methanol. This reaction required a 3-day reflux period followed by several extractions to ensure any by-product was removed. Production of this ligand gave a moderate yield of 63%. Throughout the synthesis, there were routine NMR checks to confirm the presence of the Tpm ligand. The NMR data for this ligand is shown in the **Supporting Information.**

3.5: Synthesis of Transition Metal Tpm Complexes

Furthermore, the synthesized ligand was then reacted with first-row transition metals to achieve the final desired complexes under study. The ligand was stirred in a solution containing degassed methanol with first-row transition metal chlorides. To ensure complete metalation of the Tpm ligand, the reactions were carried out overnight at room temperature. Due to the possibility of oxidizing the M^{2+} to the M^{3+}, all reactions were carried out under a nitrogen atmosphere. Partial characterization of these complexes was achieved – HRMS, CV, and solubility properties.

3.6: Characterization of Transition Metal Tpm Complexes

The first-row transition metals under study are manganese, iron, cobalt, and nickel. However, only the iron complex was redox-active within the parameters required of DSSCs. The electrochemical properties of iron(II)-bis[tris(pyrazolyl)methane] matched literature values.[19] Cyclic voltammetry was performed in the same setup as stated for the Tp complexes with the exception of acetonitrile as the supporting electrolyte. The iron$^{3+/2+}$ redox couple in acetonitrile

exhibits a chemically reversible oxidation at 1.1 V vs. Ag/AgCl and 0.69 V vs. $Fc^{+/0}$. The redox potential of this $[Fe(Tpm)_2]^{3+/2+}$ is within the desired parameter of 0.6-1.5 V vs. $Fc^{+/0}$, with a key interest on remaining close to the minimum redox potential. The solubility of $[Fe(Tpm)_2]^{3+/2+}$ exceeded the 0.25 M for application in DSSCs. Given the reversible oxidation seen at 0.69 V vs. $Fc^{+/0}$ and higher solubility, this complex could potentially yield efficiencies similar to $[Co(bpy)_3]^{3+/2+}$.

4. Conclusion

This study presents the synthesis of a tridentate tris(pyrazolyl)borate ligand to be used in first-row transition metal complexes as potential redox shuttles in DSSCs. The synthesis of the Tp ligand and metalation of this ligand were accomplished effectively. Electrochemical studies proved the viable electrochemical reversibility, yet the solubility with three tunable positions on the ligand did not yield appropriate solubilities for DSSC application. Therefore, the study explored the synthesis of a tris(pyrazolyl)methane ligand to be used in the generation of an iron complex for use as a redox shuttle in a DSSC. The synthesis of the Tpm ligand and metalation of this ligand were achieved successfully as well. Electrochemical studies indicate that the iron complex displays a reversible redox couple and solubility in acetonitrile exceeding 0.25 M as needed for the DSSC application. Given the reversibility, solubility, and potentially lower recombination than $[Co(bpy)_3]^{3+/2+}$, these properties support the hypothesis that this complex could operate efficiently as a redox shuttle. More electrochemical tests must be conducted to determine the usefulness of this potential redox mediator for DSSCs. Furthermore, pairing this complex to a particular dye and testing in a DSSC must be achieved to determine the maximum efficiency. Additionally, this ligand was unsubstituted; therefore, further analysis of the addition of electron-donating and -withdrawing groups to optimize the complex's properties and redox potential can be explored.

5. References

1. History of Energy Consumption in the United States, 1775-2009. *Today in Energy* **2011**.
2. Shafiee, S., & Topal, E. When will fossil fuel reserves be diminished? *Energy Policy*. **2009**, *37*(1), 181–189. https://doi-org /10.1016/j.enpol.2008.08.016
3. Ekwurzel, B.; Boneham, J.; Dalton, M.; Heede, R.; Mera, R.; Allen, M.; Frumhoff, P. The Rise in Global Atmospheric CO2, Surface Temperature, and Sea Level from Emissions Traced to Major Carbon Producers. *Climatic Change* **2017**, *144* (4), 579–590.
4. Jones, G.; Warner, K. The 21st Century Population-Energy-Climate Nexus. *Energy Policy* **2016**, *93*, 206–212.
5. Hydropower Explained. *U.S. Energy Information Administration* **2020**.
6. Advantages and Challenges of Wind Energy. *Wind Vision Report* **2020**.
7. Kannan, N.; Vakeesan, D. Solar Energy for Future World: - A Review. *Renewable and Sustainable Energy Reviews* **2016**, *62*, 1092–1105.
8. Solar Energy in the United States. *Energy Efficiency & Renewable Energy* **2020**.
9. Bignozzi, C.; Argazzi, R.; Boaretto, R.; Busatto, E.; Carli, S.; Ronconi, F.; Caramori, S. The Role of Transition Metal Complexes in Dye Sensitized Solar Devices. *Coordination Chemistry Reviews* **2013**, *257* (9-10), 1472–1492.
10. Sadava, D. E.; Hillis, D. M.; Heller, H. C.; Berenbaum, M. undefined. *Life: the science of biology*; Sinauer: Sunderland, MA, **2014**.
11. Alwis, D. C. L. D.; Schultz, F. A. Metal−Bis[Poly(Pyrazolyl)Borate] Complexes. Electrochemical, Magnetic, and Spectroscopic Properties and Coupled Electron-Transfer and Spin-Exchange Reactions. *Inorganic Chemistry* **2003**, *42* (11), 3616–3622.

12. Haring, A. J.; Pomatto, M. E.; Thornton, M. R.; Morris, A. J. MnII/III Complexes as Promising Redox Mediators in Quantum-Dot-Sensitized Solar Cells. *ACS Appl. Mater. Interfaces* **2014**, *6*(17), 15061-15067.
13. Hillier, A.; Zhang, X.; Maunder, G.; Liu, S.; Eberspacher, T.; Metz, M.; Mcdonald, R.; Domingos, Â.; Marques, N.; Day, V.; Sella, A.; Takats, J. Synthesis and Structural Comparison of a Series of Divalent Ln(TpR,R‘)2(Ln = Sm, Eu, Yb) and Trivalent Sm(TpMe2)2X (X = F, Cl, I, BPh4) Complexes. *Inorganic Chemistry* **2001**, *40* (20), 5106–5116.
14. Mathew, S.; Yella, A.; Gao, P.; Humphry-Baker, R.; Curchod, B.; Ashari-Astani, N.; Tavernelli, I.; Rothlisberger, U.; Nazeeruddin, M.; Grätzel, M. Dye-Sensitized Solar Cells with 13% Efficiency Achieved through the Molecular Engineering of Porphyrin Sensitizers. *Nature Chemistry* **2014**, *6* (3), 242–247.
15. Trofimenko, S. Polypyrazolylborates, a New Class of Ligands. *Accounts of Chemical Research* **1971**, *4* (1), 17–22.
16. Conde, A.; Vilella, L.; Balcells, D.; Díaz-Requejo, M.; Lledós, A.; Pérez, P. Introducing Copper as Catalyst for Oxidative Alkane Dehydrogenation. *Journal of the American Chemical Society* **2013**, *135* (10), 3887–3896.
17. Harding, D.; Harding, P.; Daengngern, R.; Yimklan, S.; Adams, H. Synthesis and Characterization of Redox-Active Tris(Pyrazolyl)Borate Cobalt Complexes. *Dalton Transactions* **2009**, 8, 1314-1320.
18. Trofimenko, S. Recent advances in poly(pyrazolyl)borate (scorpionate) chemistry. *Chem. Rev.* **1993**, 93, 943−980.

19. Sheets, J. R., Schultz, F. A.; Coupled electron-transfer and spin-exchange reactions of metal–bis[tris(pyrazolyl)methane] complexes. *Polyhedron*. **2004,** *23*(6), 1037–1043.
20. Sun, Z., Liang, M.; Chen, J. Kinetics of Iodine-Free Redox Shuttles in Dye-Sensitized Solar Cells: Interfacial Recombination and Dye Regeneration. *Accounts of Chemical Research* **2015,** *48*(6), 1541–1550.
21. Włodarczyk, A.; Richardson, R.; Ward, M.; Mccleverty, J.; Hursthouse, M.; Coles, S. Complexes of Tris(3,5-Dimethylpyrazolyl)Borates Alkylated on the 4-Position of the Pyrazolyl Rings. X-Ray Crystal Structure of Molybdenum Dicarbonyl Nitrosyl Tris(3,5-Dimethyl-4-n-Butylpyrazolyl)Borate. *Polyhedron* **1996**, *15* (1), 27–35.
22. Cortijo, M.; Viala, C.; Reynaldo, T.; Favereau, L.; et al. Synthesis, Spectroelectro chemical Behavior, and Chiroptical Switching of Tris(β-Diketonato) Complexes of Ruthenium(III), Chromium(III), and Cobalt(III). *Inorganic Chemistry* **2017**, *56* (8), 4555–4567.
23. Wang, Y.; Liu, M.; Cao, R.; Zhang, W. A Soluble Bis-Chelated Gold(I) Diphosphine Compound with Strong Anticancer Activity and Low Toxicity. *Journal of Medicinal Chemistry* **2013**, *56* (4), 1455–1466.
24. Reger, D. L.; Grattan, T.; Brown, K. J.; Little, C. A. Syntheses of Tris(Pyrazolyl)Methane Ligands and {[Tris(Pyrazolyl)Methane]Mn(CO)3}SO3CF3 Complexes: Comparison of Ligand Donor Properties. *Journal of Organometallic Chemistry* **2000**, *607* (1-2), 120–128.
25. Fisher, A. C.; Peter, L. M.; Ponomarev, E. A.; Walker, A. B.; Wijayantha, K. G. U. Intensity Dependence of the Back Reaction and Transport of Electrons in Dye-Sensitized

Nanocrystalline TiO2Solar Cells. *The Journal of Physical Chemistry B* **2000**, *104* (5), 949–958.

26. Zamponi, S.; Gambini, G.; Conti, P.; Lobbia, G.; Marassi, R.; Berrettoni, M.; Cecchi, P. Electrochemical, Spectroelectrochemical and X-Ray Absorption Spectroscopic Study of Some Iron(II) and Iron(III) Polypyrazolylborato Complexes. *Polyhedron* **1995**, *14* (13-14), 1929–1935.
27. Trofimenko, S. Boron-Pyrazole Chemistry. II. Poly(1-Pyrazolyl)-Borates. *Journal of the American Chemical Society* **1967**, *89* (13), 3170–3177.

6. Supporting Information

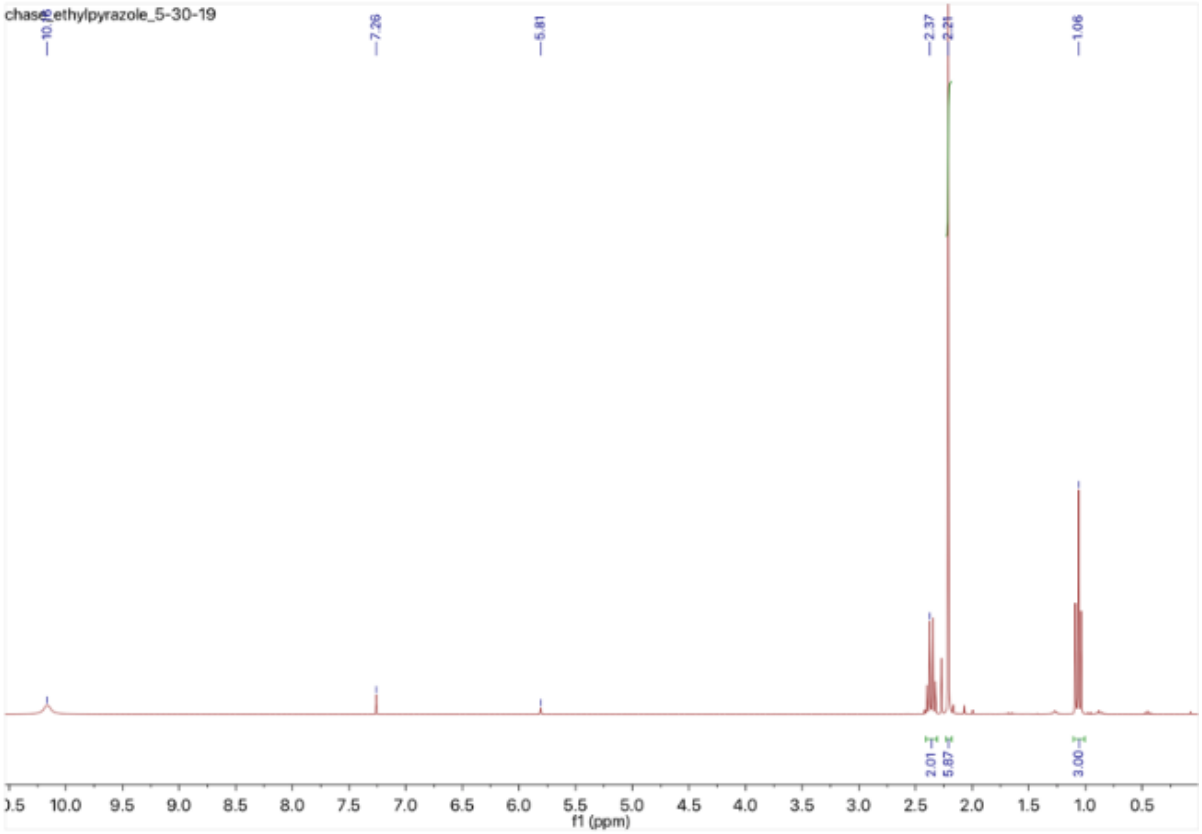

Figure 17. ^{1}H NMR ($CDCl_3$) of 3,5-dimethyl-4-ethylpyrazole.

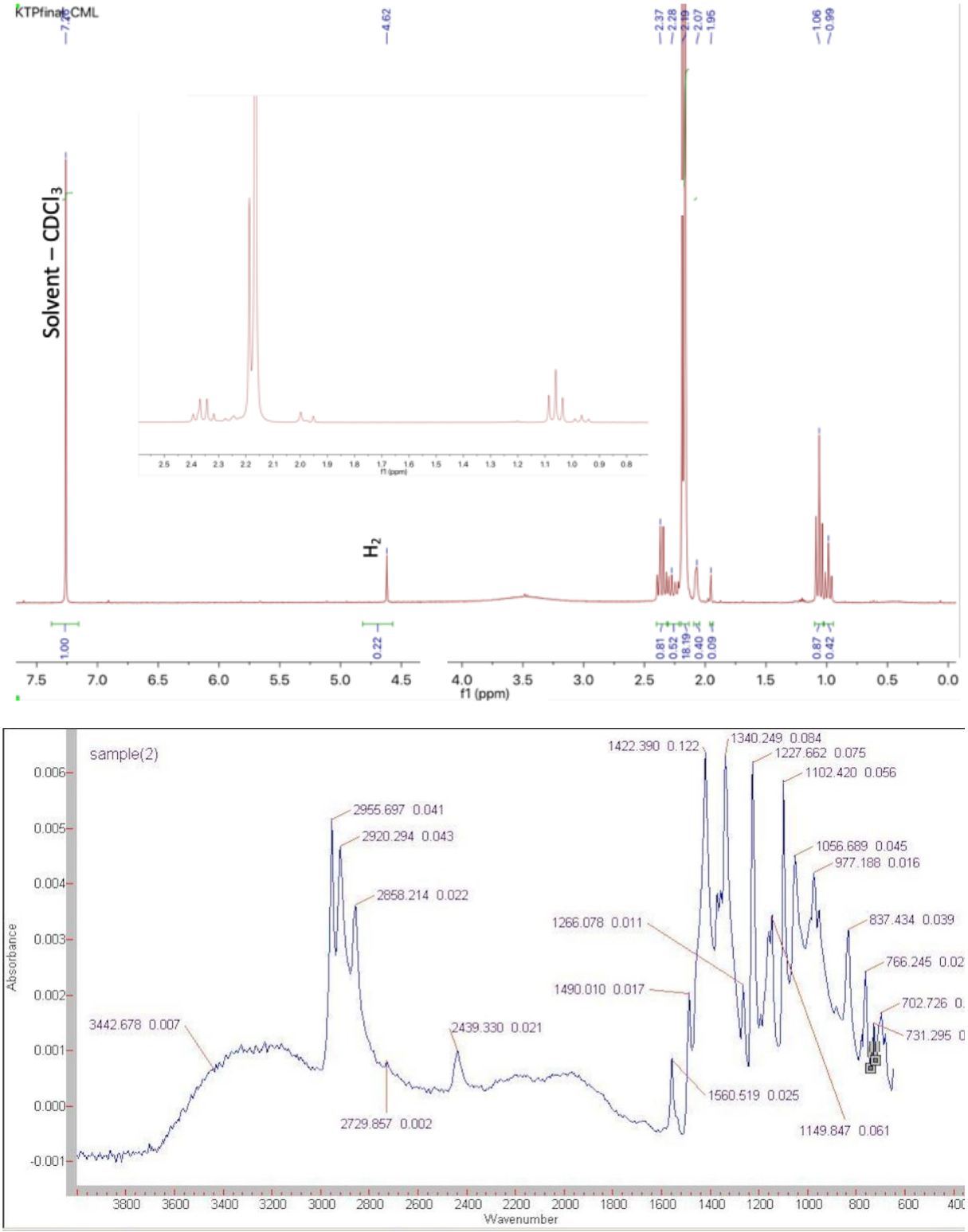

Figure 18 & 19. 1H NMR ($CDCl_3$) and FT-IR of Potassium tris(3,5-dimethyl-4-ethylpyrazolyl) borate.

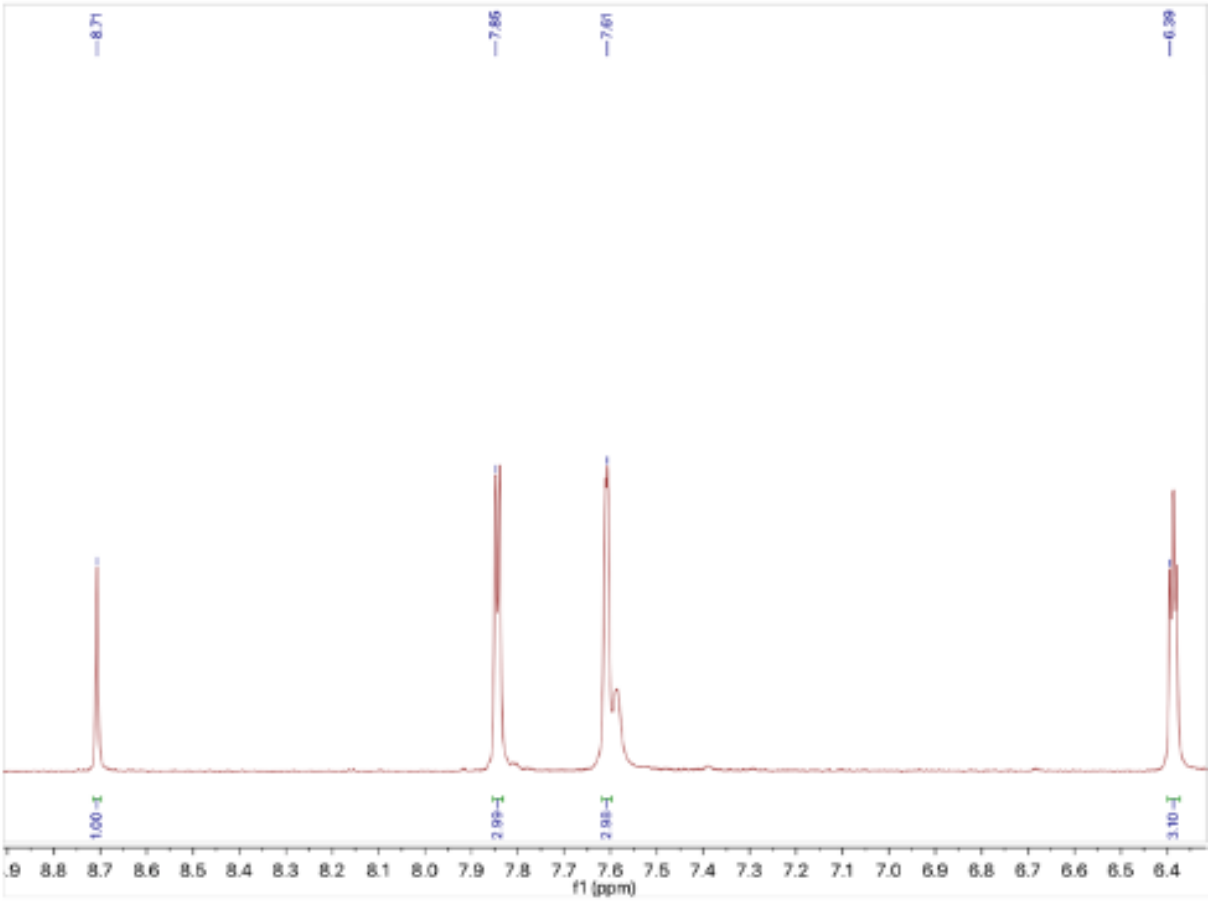

Figure 20. ^{1}H NMR (acetone-*d*$_6$) of Tris(pyrazolyl)methane.